# Oxygen rich *p*-type ZnO thin films using wet chemical route with enhanced carrier concentration by temperature-dependent tuning of acceptor defects

Usman Ilyas,[1,2] R. S. Rawat,[1,a)] T. L. Tan,[1] P. Lee,[1] R. Chen,[3] H. D. Sun,[3] Li Fengji,[4] and Sam Zhang[4]

[1]*NSSE, NIE, Nanyang Technological University, 1 Nanyang Walk, Singapore 637616*
[2]*Department of Physics, University of Engineering & Technology, Lahore, Pakistan 54890*
[3]*Division of Physics and Applied Physics, School of Physical and Mathematical Sciences, Nanyang Technological University, Singapore 637371*
[4]*School of Mechanical and Aerospace Engineering, Nanyang Technological University, 50 Nanyang Avenue, Singapore 639798*

(Received 13 June 2011; accepted 7 October 2011; published online 11 November 2011)

This paper reports the temperature-dependent tailoring of acceptor defects in oxygen rich ZnO thin films, for enhanced *p*-type conductivity. The oxygen rich *p*-type ZnO thin films were successfully grown by pulsed laser deposition on silicon substrate at different postdeposition annealing temperatures (500–800 °C). The oxygen rich ZnO powder was synthesized by wet chemical method using zinc acetate dihydrate [$Zn(CH_3COO)_2{\cdot}2H_2O$] and potassium hydroxide (KOH) as precursors. The powder was then compressed and sintered to make pellets for pulsed laser deposition system. The x-ray diffraction analysis exhibits an improved crystallinity in thin films annealed at elevated temperatures with a temperature-dependent variation in lattice constants. An analysis of Auger Zn $L_3M_{4,5}M_{4,5}$ peak reveals a consistent decrease in interstitial zinc ($Zn_i$) exhibiting its temperature-dependent reversion to zinc lattice sites. Room temperature photoluminescence of the *p*-type ZnO shows a dominant deep level emission peak at ~3.12 eV related to oxygen interstitials (acceptors). The relative concentration of oxygen interstitials ($O_i$) increases with increase in annealing temperature, resulting in enhanced hole carrier concentration. The maximum hole carrier concentration of $6.8 \times 10^{14}$ $cm^{-3}$ (indicating *p*-type conductivity) was estimated using Hall probe measurements for the thin film sample annealed at 700 °C. © *2011 American Institute of Physics*. [doi:10.1063/1.3660284]

## I. INTRODUCTION

ZnO is a promising material for various technological applications by virtue of its unique combination of piezoelectric, electrical, and optical properties. It has attracted a lot of research interest due to its exciton binding energy (60 meV) that is 2.4 times the binding energy of GaN (25 meV) and also because of its wide bandgap of 3.37 eV which make it useful for applications in various fields such as transparent conductive films, solar cells, photoconductors, and luminescence devices.[1] However, one of the main obstacles in creating high quality ZnO-based optoelectronic devices is the unavailability of highly *p*-type ZnO thin films with significant hole carrier concentration. The main reason behind the difficulty in achieving *p*-type conductivity is the presence of native defects such as oxygen vacancies and zinc interstitials which are unintentionally introduced during growth making undoped ZnO inherently an *n*-type material. A number of groups[2–6] have tried to address this issue by using various thin film growth methods and by using various Group V elements (N, P, As, and Li) as dopants. However, the stability and reproducibility of *p*-type ZnO thin films are still a matter of great concern.[7] Deep acceptor levels, low dopant solubility and high self-compensation in ZnO thin films are thought to be a bottleneck for their *p*-type conductivity.[8] There are also a few reports[9–11] on the growth of undoped *p*-type ZnO thin films in oxygen rich environment. In these reports, the thin film growth took place in optimized partial pressure of oxygen to ensure *p*-type conductivity of acceptor defects in order to overcome oxygen vacancy defects in deep level emission (DLE) spectrum, since oxygen vacancy is well-known intrinsic donor defect of ZnO. Therefore, it is worthwhile to synthesize and investigate oxygen rich ZnO to improve the intrinsic *p*-type behavior of ZnO thin films without adopting any doping method or oxygen partial pressure.

In this paper, we report the synthesis and investigation of oxygen rich ZnO thin films using wet chemical method (favorable to form undoped *p*-type ZnO) without using any oxygen rich environment or acceptor dopant during ZnO thin film growth. Temperature-dependent tailoring of acceptor defects has also been carried out to investigate their contribution toward *p*-type conductivity. It is well known that the properties of ZnO layers are strongly affected not only by growth conditions but also by postdeposition annealing temperatures. Annealing has a large effect on crystallinity of layers in terms of grain size, residual strain, and defect density.[12] So, it is valuable to investigate the intrinsic *p*-type behavior of pulsed laser deposition (PLD) grown ZnO thin films by tuning the acceptor defects with postdeposition annealing.

[a)]Electronic mail: rajdeep.rawat@nie.edu.sg.

 © 2011 American Institute of Physics

Author complimentary copy. Redistribution subject to AIP license or copyright, see http://apl.aip.org/apl/copyright.jsp

## II. EXPERIMENTATION

### A. Preparation of nanocrystalline ZnO powder for PLD pellet

Nanosrystalline ZnO powder, used for preparing PLD pellets, with wurtzite structure was synthesized through a wet chemical method by a chemical reaction of 90 mMol zinc acetate dihydrate [$Zn(CH_3COO)_2 \cdot 2H_2O$] and 280 mMol potassium hydroxide (KOH) in an environment of 800 ml of methanol. The solution was continuously stirred magnetically (1100 rev/min) and heated at 52 °C for 3 h. The solution was allowed to cool and aged at room temperature for 24 h. Precipitates formed after aging were removed from the solution by filtration. The precipitates washed several times with distilled water were centrifuged (2000 rev/min) to get rid of potassium completely from the solution. The precipitates were dried at 52 °C in air to get solid powder. The powder obtained was pelletized under a pressure of 10.5 metric tons and sintered at ~1000 °C for 12 h in air. It is important to point out that the x-ray photoelectron spectroscopy (XPS) analysis of the ZnO powder prepared by wet chemical method was oxygen rich with Zn/O ratio of 0.71.

### B. ZnO thin film deposition using PLD

The sintered pellet of ZnO (circular disk of 20 mm diameter and 2 mm thickness) was fixed on the target holder of the PLD system and rotated at 33 rev/min for uniform ablation. The rotating target was then ablated by second harmonic Nd:YAG laser (532 nm, 26 mJ) at pulse repetition rate of 10 Hz. The substrate holder was rotated at 33 rev/min to ensure uniform deposition of thin films. The thin films were deposited on Si (100) substrate for constant ablation duration of 90 min in ultra high vacuum of $10^{-6}$ Torr. The Si (100) substrates were sequentially cleaned in ultrasonic bath with ethanol, acetone, and deionized water separately at 45 °C for 15 min each, before being mounted to the substrate holder in the PLD chamber. Postdeposition annealing was carried out at different temperatures ranging from 500 to 800 °C for 4 h in air.

The crystalline phase of thin films was analyzed using SIEMENS D5005 Cu Kα (1.504 Å) x-ray Diffractometer (XRD). The surface stoichiometry and elemental oxidation states of the thin films were identified by x-ray photoelectron spectroscopy (XPS) with Kratos axis-ultra spectrometer equipped with a focused monochromatic Al-Kα x-ray beam at room temperature. Furthermore, near band edge (NBE) and deep level emission (DLE) energy transitions from photoluminescence (PL) spectra, measured using Hd-Cd (325 nm, 10 mW), were used to study temperature-dependent activation of structural defects in ZnO thin films. The electrical properties of the thin films were investigated by Van der Pauw method using Ecopia HMS-3000 Hall effect measurement system. The surface morphologies of the thin films were investigated using Jeol JSM 6700 field emission scanning electron microscope (FESEM).

## III. RESULTS AND DISCUSSION

XRD spectra of postannealed ZnO thin films grown by PLD are shown in Fig. 1. The diffraction peaks of ZnO observed in the 2$\theta$ range from 20° to 80° exhibited polycrystalline wurtzite structure for all annealed thin films. The XRD spectra obtained are matched well with the space group of $P_63mc$ (186) and diffraction peaks corresponding to any impurity phase were not detected. The diffraction peak intensities, revealing the crystallinity of ZnO thin films, were continuously improved with increasing postdeposition annealing temperature without any degradation in crystalline quality, in the used temperature range, in accordance with reported literature.[13,14] Highly textured peak centered at ~36.29° (characterizing the hexagonal wurtzite structure) shifted toward larger angles with the increase in annealing temperature from 500 to 800 °C, as shown in Fig. 2. This peak shift toward larger angles is attributed to the activation of certain point defects and rearrangement of crystal grains.[15] The crystallite size estimated from the full width at half maximum (FWHM) of (101) diffraction peak, using the Scherer equation and shown in Fig. 2, increased from 18.2 to 26.6 nm with the increase in annealing temperature from 500 to 800 °C, illustrating improved crystalline quality.[16]

The defect formation has been verified by change in lattice parameters as a function of annealing temperature. The

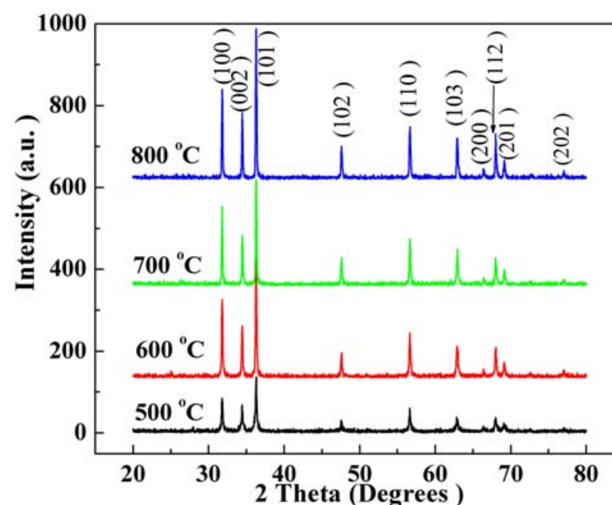


FIG. 1. (Color online) XRD spectra of PLD grown ZnO thin films annealed at temperatures of 500, 600, 700, and 800 °C.

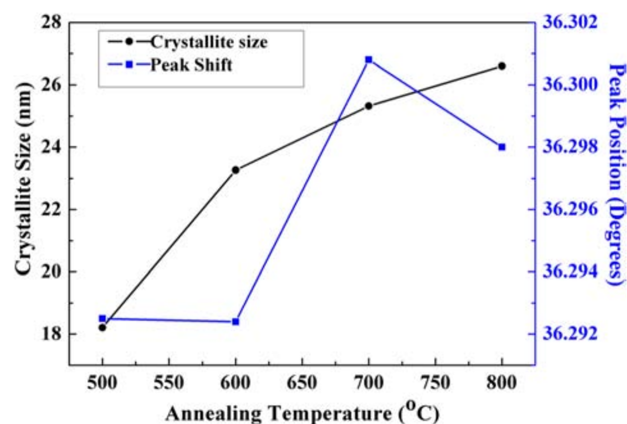


FIG. 2. (Color online) Variation in the position of (101) diffraction peak and the average crystallite size of ZnO thin films with the increase in annealing temperature from 500 to 800 °C.

Author complimentary copy. Redistribution subject to AIP license or copyright, see http://apl.aip.org/apl/copyright.jsp

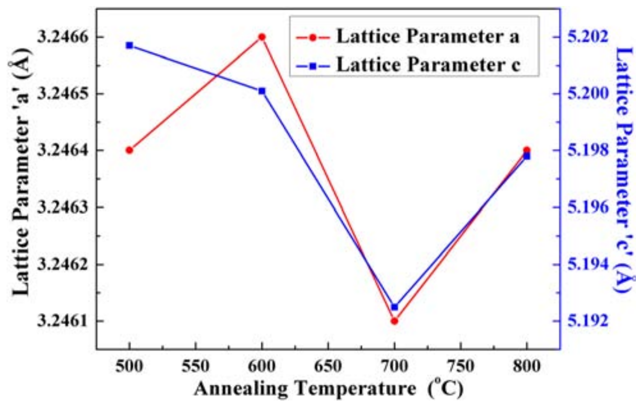


FIG. 3. (Color online) Variation in lattice parameters "a" and "c", estimated from (101) and (002) diffraction peaks, of ZnO thin films with the increase in the annealing temperature from 500 to 800 °C.

lattice parameters $a$ and $c$, calculated by using diffraction data of (101) and (002) peaks, were higher than those reported in literature ($a = 3.2427$ Å and $c = 5.1948$ Å) for ZnO.[17] Figure 3 shows the temperature-dependent variation in lattice constants. This might be attributed to the variation in tensile/compressive stresses of ZnO coated silicon wafer due to the activation of certain point defects at different annealing temperatures. The detailed analysis of temperature-dependent behavior of lattice parameters in terms of point defects such as zinc and oxygen interstitials will be discussed later using XPS and PL results.

The FESEM images, depicting the surface morphologies, of the thin film samples annealed at different temperatures are shown in Fig. 4. All the thin films exhibit well-defined grains with similar surface features. At first glance, it seems that the change in the annealing temperature does not affect the surface features. However, a careful processing of the FESEM images (using ImageJ® software) reveals that for the sample annealed at 500 °C the average grain size distribution is bi-modal in nature with the average grain size of smaller grains as $52 \pm 2.8$ nm and that of bigger grains as $192 \pm 5.1$ nm. The increase in annealing temperature to 600 °C leads to greater uniformity in grain size distribution due to the significant reduction in the number of smaller sized grains as they start to coalesce together to form bigger grains. A further increase in annealing temperature (to 700 and 800 °C) made the grains to be more uniform in size with slight increase in grain size.

The typical XPS survey scan of as-deposited thin films, shown in Fig. 5, exhibits the presence of zinc and oxygen as the main elements with their binding energies being calibrated by adventitious $C$ 1s peak centered at 284.6 eV. The stoichiometery of as-deposited thin films (without annealing) is found to be oxygen rich with $Zn/O = 0.49$, that is different from the literature in which the stoichiometery is reported to be zinc rich.[18,19] The direct synthesis of oxygen rich ZnO thin film (as-deposited) can be attributed to the fact that the PLD pellet of ZnO, prepared using the wet chemical method, itself was oxygen rich. So even without any partial oxygen pressure being used in PLD chamber, the oxygen rich ZnO thin films were grown. Similar XPS spectra were obtained for the annealed thin film samples and the relative concentration of Zn and O was estimated. Figure 6 shows the plot of Zn and O concentrations along with their difference in concentration as a function of thin film annealing temperature. It

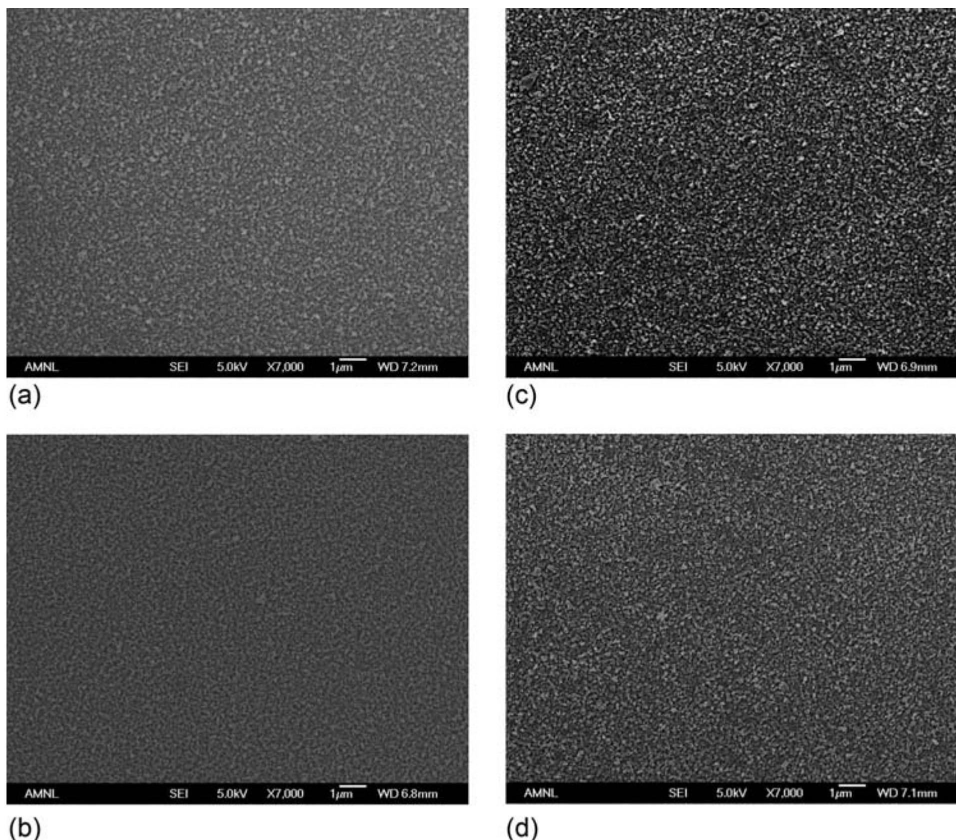


FIG. 4. FESEM micrographs of ZnO thin films annealed at (a) 500 °C, (b) 600 °C, (c) 700 °C, and (d) 800 °C.

Author complimentary copy. Redistribution subject to AIP license or copyright, see http://apl.aip.org/apl/copyright.jsp

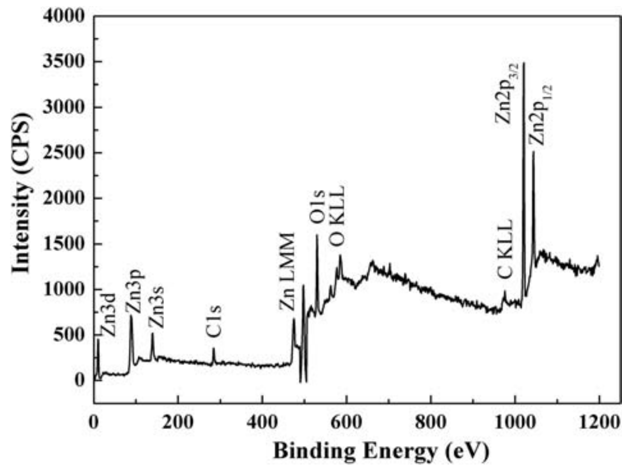


FIG. 5. The typical XPS survey scan spectrum, calibrated using adventitious *C* 1s peak centered at ∼284.6 eV, of as-deposited ZnO thin film showing the presence of oxygen, zinc, and carbon.

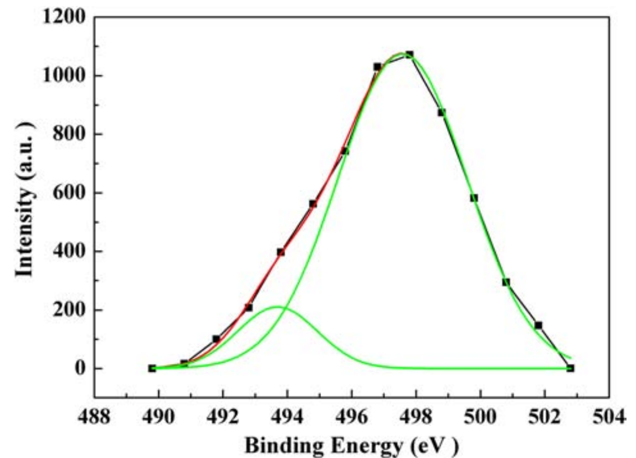


FIG. 7. (Color online) The Zn LMM Auger spectrum of ZnO thin film annealed at 700 °C which is deconvoluted, using Gaussian peak fitting, with two peaks centered at ∼493.8 and ∼497.5 eV.

indicates that the oxygen concentration is much higher than the zinc concentration pointing out that the stoichiometery of ZnO remains oxygen rich even in the annealed samples. Moreover, the zinc concentration decreases with annealing temperature up to 700 °C and increases again at 800 °C. The minimum concentration of Zn at 700 °C will also result in the contraction of lattice ultimately leading to the minimum lattice parameters of ZnO thin films that is consistent with our XRD results.

Since Zn $2p3/2$ peak shape does not always give an asymmetric feature, so the Zn *LMM* Auger peak analysis is often used to identify the chemical states of the zinc species. Auger peaks usually show larger shape changes than XPS peaks with varying chemical states because a single Auger transition involves three electrons and many body effects.[20] Figure 7 shows the typical Auger Zn $L_3M_{4,5}M_{4,5}$ spectrum of the ZnO thin films for the sample annealed at 700 °C. This spectrum is Gaussian fitted with two Auger peaks centered at ∼493.8 and 497.5 eV which are attributed to the interstitial zinc ($Zn_i$) and Zn–O bonds, respectively.[7] The concentration of the $Zn_i$ and Zn–O bonds are estimated using the relative area under the corresponding deconvoluted Auger peaks. The variations in relative concentrations of $Zn_i$ and Zn–O bonds, at annealing temperatures of 500, 600, 700, and 800 °C are shown in Fig. 8. The $Zn_i$ atoms in as-deposited ZnO thin films, usually located between $O^{2-}$ and $Zn^{2+}$ layers, are responsible for increase in lattice constants. During annealing, zinc interstitials are reported to obtain enough energy to revert back to crystal lattice sites after recombination with zinc vacancies resulting in strong Zn–O bonding[21] as is evident from Fig. 8. The concentration of $Zn_i$ first decreases with increasing annealing temperature, having minimum value at 700 °C, and then increases when annealed at 800 °C. The increased concentration of $Zn_i$ at 800 °C can be attributed to the large number of zinc vacancies which are reported to be formed at elevated temperatures.[22] This variation in $Zn_i$ is responsible for the contraction/expansion of crystal lattice at different annealing temperatures. The minimum value of $Zn_i$ at 700 °C is responsible for the contraction of lattice at this temperature resulting in reduced lattice parameters as is evident from Fig. 3. Since the $Zn_i$ is donor impurity, so the reduced concentration of $Zn_i$ at 700 °C is

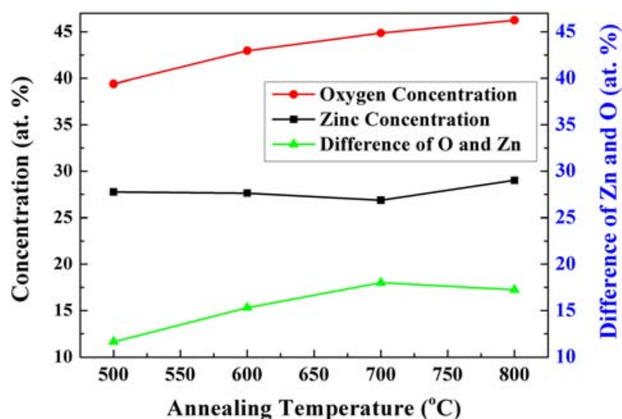


FIG. 6. (Color online) A plot of Zn and O atomic concentrations estimated from the relative area under their XPS peaks after a Shirley background subtraction by nonlinear least square fitting using mixed Gauss-Lorentz function along with their differences at different annealing temperatures (500–800 °C).

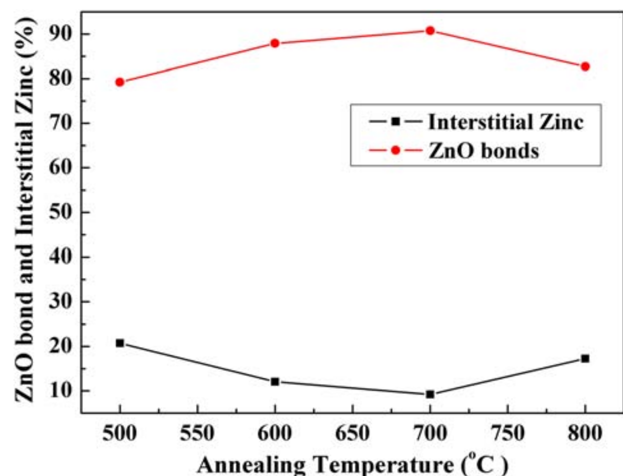


FIG. 8. (Color online) Variation in concentration of interstitial zinc and Zn–O bonds with the increase in annealing temperature from 500 to 800 °C.

Author complimentary copy. Redistribution subject to AIP license or copyright, see http://apl.aip.org/apl/copyright.jsp

TABLE I. Carrier concentration, resistivity, and carrier mobility of undoped *p*-type ZnO thin films.

| Postdeposition annealing | Hole concentration ($cm^{-3}$) | Resistivity ($\Omega$ cm) | Carrier mobility ($cm^2\ V^{-1}\ s^{-1}$) |
|---|---|---|---|
| 500 °C | $9.52 \times 10^{11}$ | $2.54 \times 10^{5}$ | $2.58 \times 10^{1}$ |
| 600 °C | $2.60 \times 10^{12}$ | $6.65 \times 10^{3}$ | $3.60 \times 10^{2}$ |
| 700 °C | $6.80 \times 10^{14}$ | $1.89 \times 10^{2}$ | $1.75 \times 10^{3}$ |
| 800 °C | $4.60 \times 10^{12}$ | $7.40 \times 10^{2}$ | $9.88 \times 10^{2}$ |

favorable to form undoped *p*-type ZnO useful for optoelectronic applications.

In order to validate our argument regarding formation of undoped *p*-type ZnO, Hall probe measurements of annealed ZnO thin films were performed using Van der Pauw method to characterize their electrical properties. The Hall probe measurements are summarized in Table I which shows that the conductivity of ZnO thin films is *p*-type with the minimum hole carrier concentration ($\sim 9.5 \times 10^{11}$ $cm^{-3}$) in the thin film annealed at 500 °C and maximum ($\sim 6.8 \times 10^{14}$ $cm^{-3}$) in thin film annealed at 700 °C. The *p*-type conductivity in the annealed samples can be attributed to oxygen rich ($Zn/O < 1$) stoichiometery, for all the thin film samples. The increase in hole carrier concentration with the increase in temperature is due to increasing difference between the oxygen and zinc concentration (refer Fig. 6). The maximum difference between the oxygen and the zinc concentration for the thin film annealed at 700 °C explains the maximum *p*-type conductivity for this sample. Hence, it is found that the *p*-type conductivity in undoped ZnO thin films can be obtained using oxygen rich powder synthesized by wet chemical method and can also be further enhanced by tailoring the postdeposition annealing temperature. This is different from previously reported methodologies[9–11] in which the *p*-type ZnO was realized using oxygen rich environment in growth chambers or by selective doping.

The asymmetric *O* 1s XPS peak was deconvoluted with peaks centered at 530.3 and 531.7 eV for all the annealed thin film samples. The typical deconvoluted *O* 1s peak for the sample annealed at 500 °C is shown in Fig. 9. The results are almost similar to Chen *et al.*[23] and Wang *et al.*[24] who attributed 530 eV peak to Zn–O bonds. The higher binding energy (531.7 eV) peak is usually attributed to chemisorbed or dissociated oxygen or hydroxyl (OH) species on the surface of the ZnO thin film.[25] The component of binding energy centered at 531.0 eV in thin films annealed at higher temperature (700 and 800 °C) is associated with the $O^{2-}$ ions which are in oxygen deficient regions within the ZnO matrix. As a result, changes in the intensity of this component are related to the variation in the concentration of the oxygen vacancies ($V_o$)[26] at elevated temperatures.

Figure 10 shows the room temperature PL spectrum of ZnO thin films annealed at 700 °C exhibiting UV and defect (green) emission. UV band emission centered at ~383 nm, is originated from the exciton recombination corresponding to the near band edge (NBE) exciton emission of the wide bandgap ZnO. These recombinations take place through exciton–exciton collision processes at room temperature.[27] The deep level emissions (DLE) in green and yellow emission spectra are related to the variation in intrinsic defects of ZnO thin films, such as zinc vacancy ($V_{Zn}$), oxygen vacancy ($V_o$), interstitial zinc ($Zn_i$), and interstitial oxygen ($O_i$). Various intrinsic defects in ZnO thin films exhibit different energies in DLE.[28] The DLE spectrum, as seen in Fig. 10, can be deconvoluted with four peaks centered at ~384.02 nm (3.23 eV), 490.67 nm (2.53 eV), 538.54 nm (2.31 eV), and 582.09 nm (2.13 eV). The peak related to 2.13 eV exhibits the signatures of yellow emission attributed to the $O_i$ in ZnO thin films.[29] The evaluated energy of singly ionized $Zn_i$ is 2.53 eV that is attributed to the transition from energy level of singly ionized $Zn_i$ to Zn vacancy ($V_{Zn}$) while 2.31 eV is related to oxygen vacancies ($V_o$) from the bottom of conduction band to local defect energy level. The $Zn_i$ is donor impurity while $O_i$ and $V_{Zn}$ add acceptor levels to ZnO thin films. Most of the calculations agree that $V_o$ and $V_{Zn}$ are the lowest energy defects, while the zinc and oxygen interstitials to be high in energy. The defects which are favored under Zn-rich conditions ($V_o$, $Zn_i$) act as donors, while those favored under O-rich conditions ($V_{Zn}$, $O_i$) act as acceptors.[30] Table II shows the variation in relative concentrations of zinc (donor) and oxygen (acceptor) interstitials as estimated from deconvoluted PL

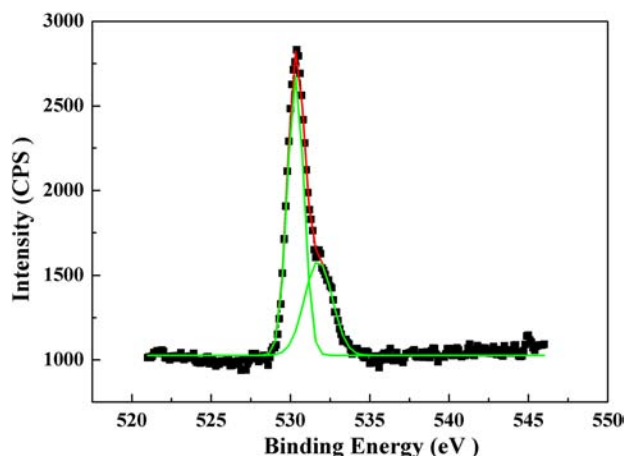


FIG. 9. (Color online) *O* 1s core level XPS spectrum (deconvoluted using two Gaussian peaks centered at ~530.3 and 531.7 eV) of ZnO thin film annealed at 500 °C.

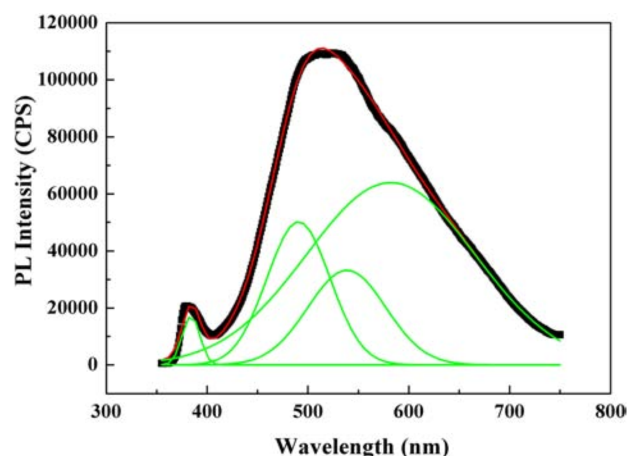


FIG. 10. (Color online) Deconvoluted room temperature PL spectrum (comprising of near band edge and deep level emission bands) of ZnO thin film annealed at 700 °C.

Author complimentary copy. Redistribution subject to AIP license or copyright, see http://apl.aip.org/apl/copyright.jsp

TABLE II. Relative concentration of oxygen and zinc interstitials estimated from PL emission spectra.

| Postdeposition annealing | Zinc interstitials ($Zn_i$ %) | Oxygen interstitials ($O_i$ %) |
|---|---|---|
| 500 °C | 45.04 | 54.95 |
| 600 °C | 37.21 | 62.78 |
| 700 °C | 32.90 | 67.09 |
| 800 °C | 37.78 | 62.21 |

spectra. The relatively higher concentration of $O_i$ (acceptor defect) compared to that of $Zn_i$ (donor defects) results in observed *p*-type conductivity in the annealed samples. The thin film annealed at 700 °C has minimum concentration of $Zn_i$ and maximum concentration of $O_i$ exhibiting enhanced *p*-type conductivity at this temperature.

The temperature-dependent analysis of UV peak in PL emission has also been carried out to study the effect of temperature on UV peak shift. The relative contribution of UV deconvoluted peak was increased from 1.4 to 2.7% with increase in temperature resulting in reduced DLE (defects) contribution. Therefore, it is emphasized here that dominant concentration of oxygen in all the thin films did not increase the DLE in visible range with the increase in annealing temperature that is different from the results reported in literature.[28] The UV energy shifts toward the longer wavelength (redshift) from 3.24 to 3.0 eV with the increase in temperature from 500 to 800 °C that is in agreement to the Wang *et al.*[31] who suggested an increase in wavelength (redshift) with the increase in annealing temperature. The reported typical UV peak position is at 3.26 eV.[13] This redshift can be partially explained by shrinkage of the energy bandgap with an increase in particle size as suggested by Van Dijke.[32] According to quantum confinement theory, the energy bandgap of a semiconductor depends on the particle/crystallite size; its value will decrease with a increase in particle/crystallite size. Hence in our case the decrease in energy bandgap can be attributed to the increase in average grain/crystallite size with increasing annealing temperature as inferred through XRD results.

## IV. CONCLUSION

The oxygen rich nanocrystalline ZnO powder was prepared using zinc acetate dihydrate and potassium hydroxide as precursors by simple wet chemical method instead of using commercially available zinc rich powder. The thin films of ZnO, grown by PLD and annealed at different temperatures exhibited consistent increase in average crystallite size, improved crystalline quality, and reduced optical bandgap with increase in postdeposition annealing temperature. The FESEM results indicate that surface morphologies are similar for all annealed thin film samples and the grains become more uniform with slight increase in average grain size with increasing annealing temperature. Temperature-dependent lattice parameters were calculated to be minimum at annealing temperature of 700 °C exhibiting maximum reversion of $Zn_i$ to the zinc lattice sites suggesting abundant Zn–O bonding. The detailed XPS analysis of Auger Zn $L_3M_{4,5}M_{4,5}$ peaks reveals a decrease in interstitial zinc (recombination with zinc vacancy) with increase in annealing temperature reaching to their minimum concentration at 700 °C resulting in enhanced *p*-type conductivity at this temperature. Increased concentration of oxygen interstitials in DLE spectra validated the XPS results in which all the thin films were oxygen rich. While 700 °C was observed to be optimum annealing temperature at which the relative concentration of $Zn_i$ (donor defects) was calculated to be minimum with maximum contribution of $O_i$ (acceptor defects) obliging enhanced *p*-type conductivity. To conclude, the *p*-type conductivity in PLD grown undoped ZnO thin films is obtained using a different method that employs PLD pellets of oxygen rich powder synthesized by wet chemical method; the conductivity is further enhanced by tailoring the postdeposition annealing temperature.

## ACKNOWLEDGMENTS

This project was supported by the AcRF grant (RI 7/08 RSR) provided by NIE, Nanyang Technological University, Singapore. One of the authors, Usman Ilyas, is grateful to the University of Engineering & Technology Lahore, Pakistan for providing fully funded research scholarship under faculty development program (FDP) of Higher Education Commission (HEC) of Pakistan.

[1] Q. P. Wang, D. H. Zhang, Z. Y. Xue, and X. J. Zhang, Opt. Mater. **26**, 23 (2004).
[2] S. B. Zhang, S. H. Wei, and A. Zunger, Phys. Rev. B **63**, 075205 (2001).
[3] D. C. Look, D. C. Reynolds, C. W. Litton, R. L. Jones, D. B. Eason, and G. Cantwell, Appl. Phys. Lett. **81**, 1830 (2002).
[4] D. K. Hwang, H. S. Kim, J. H. Lim, J. Y. Oh, J. H. Yang, S. J. Park, K. K. Kim, D. C. Look, and Y. S. Park, Appl. Phys. Lett. **86**, 151917 (2005).
[5] V. Vaithianathan, B. T. Lee, and S. S. Kim, Appl. Phys. Lett. **86**, 62101 (2005).
[6] Y. J. Zeng, Z. Z. Ye, W. Z. Xu, D. Y. Li, J. G. Lu, L. P. Zhu, and B. H. Zhao, Appl. Phys. Lett. **88**, 062107 (2004).
[7] G. Z. Xing, B. Yao, C. X. Cong, T. Yang, Y. P. Xie, B. H. Li, and D. Z. Shen, J. Alloys Compd. **457**, 36 (2008).
[8] Z. Z. Ye, J. G. Lu, H. H. Chen, Y. Z. Zhang, L. Wang, B. H. Zhao, and J. Y. Huang, J. Cryst. Growth **253**, 259 (2003).
[9] Y. Y. Liu, H. J. Jin, and C. B. Park, Trans. Electr. Electron. Mater. **10**, 24 (2009).
[10] M. S. Oh, S. H. Kim, and T. Y. Seong, Appl. Phys. Lett. **87**, 122103 (2005).
[11] Y. Ma, G. T. Du, S. R. Yang, Z. T. Li, B. J. Zhao, X. T. Yang, T. P. Yang, Y. T. Zhang, and D. L. Liu, J. Appl. Phys. **95**, 6268 (2004).
[12] M. Jung, J. Lee, S. Park, H. Kim, and J. Chang, J. Cryst. Growth **283**, 384 (2005).
[13] Y. Chen, D. M. Bagnall, K. T. Park, H. Koh, K. Hiraga, Z. Q. Zhu, and T. Yao, Appl. Phys. **85**, 2595 (1999).
[14] K. S. Kim, H. W. Kim, and N. H. Kim, Physica B **334**, 343 (2003).
[15] X. J. Liu, C. Song, F. Zhang, X. B. Wang, and F. Pan, J. Phys. D **40**, 1608 (2007).
[16] B. J. Jin, S. Im, and S. Y. Lee, Thin Solid Films **366**, 107 (2000).
[17] T. M. Sabine and S. Hogg, Acta Crystallogr. B **25**, 2254 (1969).
[18] Y. Zhang, G. Du, X. Yang, B. Zhao, Y. Ma, T. Yang, H. C. Ong, D. Liu, and S. Yang, Semicond. Sci. Technol. **19**, 755 (2004).
[19] P. T. Hsieh, Y. C. Chen, K. S. Kao, and C. M. Wang, Appl. Phys. A: Mater. Sci. Process. **90**, 317 (2008).
[20] J. T. Wolan and G. B. Horflund, Appl. Surf. Sci. **125**, 251 (1998).
[21] S. Dutta, M. Chakrabarti, S. Chattopadhyay, D. Sanyal, A. Sarkar, and D. Jana, J. Appl. Phys. **98**, 53513 (2005).
[22] S. Dutta, S. Chattopadhyay, D. Jana, A. Banerjee, S. Manik, S. K. Pradhan, M. Sutradhar, and A. Sarkar, J. Appl. Phys. **100**, 114328 (2006).
[23] M. Chen, X. Wang, Y. H. Yu, Z. L. Pie, X. D. Bai, C. Sun, R. F. Huang, and L. S. Wen, Appl. Surf. Sci. **158**, 134 (2000).
[24] Z. G. Wang, X. T. Zu, S. Zhu, and L. M. Wang, Phys. E **35**, 199 (2006).

Author complimentary copy. Redistribution subject to AIP license or copyright, see http://apl.aip.org/apl/copyright.jsp

[25]S. Major, S. Kumar, M. Bhatnagar, and K. L. Chopra, Appl. Phys. Lett. **49**, 394 (1986).
[26]T. Szorenyi, L. D. Laude, I. Bertoti, Z. Kantor, and Z. Geretovszky, J. Appl. Phys. **78**, 6211 (1995).
[27]L. L. Yang, Q. X. Zhao, M. Willander, J. H. Yang, and I. Ivanov, J. Appl. Phys. **105**, 53503 (2009).
[28]B. Lin, Z. Fu, and Y. Yia, Appl. Phys. Lett. **79**, 943 (2001).
[29]L. Schmidt-Mende and L. Macmanus-Driscoll, J. Mater. Today **10**, 40 (2007).
[30]A. Janotti and C. G. V. Walle, Rep. Prog. Phys. **72**, 126501 (2009).
[31]Y. G. Wang, S. P. Lau, H. W. Lee, S. F. Yu, and B. K. Tay, J. Appl. Phys. **94**, 354 (2003).
[32]A. Van Dijkin, E. A. Meulenkamp, D. Vanmaekelbergh, and A. Meijerink, J. Lumin. **90**, 123 (2000).

Author complimentary copy. Redistribution subject to AIP license or copyright, see http://apl.aip.org/apl/copyright.jsp